ISSN 0021-3640, JETP Letters, 2006, Vol. 83, No. 8, pp. 327–331. © Pleiades Publishing, Inc., 2006.

Density of States in SF Bilayers with Arbitrary Strength of Magnetic Scattering¶

D. Yu. Gusakova[a, *], A. A. Golubov[b], M. Yu. Kupriyanov[a], and A. Buzdin[c]

[a] *Institute of Nuclear Physics, Moscow State University, Moscow, 119992 Russia*

[b] *Department of Applied Physics, University of Twente, 7500 AE Enschede, The Netherlands*

[c] *Institut Universitaire de France and the Condensed Matter Theory Group, CPMOH, University Bordeaux 1, UMR 5798, CNRS, F-33405 Talence Cedex, France*

**e-mail: dariamessage@yandex.ru*

Received March 13, 2006

We developed a self-consistent method for the calculation of the density of states $N(\varepsilon)$ in SF bilayers. It is based on the quasi-classical Usadel equations and takes into account the suppression of superconductivity in the S layer due to the proximity effect of the F metal, as well as existing mechanisms of the spin dependent electron scattering. We demonstrate that the increase of the spin orbit or spin flip electron scattering rates results in completely different transformations of $N(\varepsilon)$ at the free F layer interface. The developed formalism has been applied for the interpretation of the available experimental data.

PACS numbers: 74.45.+c, 74.50.+r

DOI: 10.1134/S0021364006080066

It is well known that superconductivity can be induced into a nonsuperconducting material from a superconductor due to proximity effects. In superconductor (S)–normal metal (N) bilayers, the thus induced minigap and the shape of the density of states (DOS) at the free N metal interface $N(\varepsilon)$ depends on the values of the suppression parameters of the SN interface and the relation between the N layer thickness and the decay length of the N metal [1–4]. The existence of the minigap has been confirmed experimentally in a variety of proximity SN systems (see, e.g., [5–8] and references therein). In the superconductor–ferromagnet (F) bilayers, there are additional bulk F-layer parameters that influence $N(\varepsilon)$. They are the exchange field H and the electron spin scattering processes. The exchange field tends to align all the electron spins along the field axis. It splits the minigap and the density of states for spin up and spin down electrons (see [9–11] for reviews). The experimental study of the proximity effect in SF systems [12–16] and the Josephson effect in SFS junctions [17, 18] reveals that, besides the exchange field, the additional pair-breaking magnetic mechanism, namely, spin dependent electron scattering, should be taken into account for the data interpretation.

There are three types of spin dependent electron scattering in the ferromagnet–spin-orbit interaction and spin-flip processes that may happen along the exchange field direction and in the plane perpendicular to it. Previously, the influence of the parallel spin-flip and spin-orbit scattering mechanisms on $N(\varepsilon)$ had been considered in some limiting cases (rigid boundary conditions at SF interfaces, limits of large or small F layer thicknesses) [19, 20].

In this paper, for the first time, we developed a self-consistent method for the calculation of the density of states in SF bilayers. It is based on the quasi-classical Usadel equations and takes into account the suppression of the superconductivity in the S layer due to the proximity effect with the F metal, as well as all three mechanisms of the spin dependent electron scattering. We have demonstrated that the developed formalism can be applied for understanding the $N(\varepsilon)$ data obtained in superconductors with antiferromagnet ordering. We consider an SF bilayer consisting of two dirty metals. They are a superconductor of thickness d_s and a thin ferromagnet d_f adjoined at $x = 0$. All the physical quantities depend on the coordinate x perpendicular to the SF boundary. The exchange field is parallel to the SF interface plane. The DOS can be calculated from the Usadel equations. To proceed further, it is convenient to use the θ parameterization $G(\omega, x) = \cos\theta(\omega, x)$, $F(\omega, x) = \sin\theta(\omega, x)$, where G and F are normal and anomalous Green's functions. The magnetic and spin-orbit scattering mix up the up and down spin states, which couples the Usadel equations for the Green's functions with the opposite spin directions. In the F

¶ The text was submitted by the authors in English.

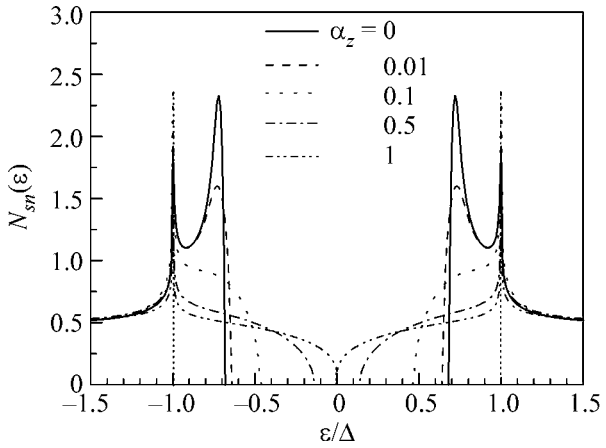

Fig. 1. The case of the parallel magnetic scattering in the S/N bilayer ($H/\pi T_c = 0$). The spin up energy DOS variation in the N layer for severed values of the magnetic scattering parameter α_z and for the fixed parameters $\gamma_B = 5$, $\gamma = 0.05$, $d_f/\xi_n = 0.2$, $d_s/\xi_s = 10$, $\alpha_x = 0$, and $\alpha_{s0} = 0$.

layer ($x < 0$), it gives the system of two equations

$$-\frac{D_f}{2}\frac{\partial^2\theta_{f1(2)}}{\partial x^2} + \left(\omega \pm iH + \frac{1}{\tau_z}\cos\theta_{f1(2)}\right)\sin\theta_{f1(2)} + \frac{1}{\tau_x}\sin(\theta_{f1} + \theta_{f2}) \pm \frac{1}{\tau_{so}}\sin(\theta_{f1} - \theta_{f2}) = 0, \quad (1)$$

and in the S layer ($x > 0$) the Usadel equations stay uncoupled

$$-\frac{D_s}{2}\frac{\partial^2\theta_{s1(2)}}{\partial x^2} + \omega\sin\theta_{s1(2)} = \Delta(x)\cos\theta_{s1(2)}, \quad (2)$$

where θ_1 and θ_2 correspond to the Green's functions with the opposite spin directions; $\omega = \pi T(2n + 1)$ are the Matsubara frequencies; $D_s(D_f)$ is the diffusion coefficient in the S (F) layer; H is the exchange field energy in the F layer; and $\Delta(x)$ is the superconducting energy gap, which is zero in the F layer. Here, we use the self-consistent method to resolve the Usadel equations, which takes into account the decrease of the energy gap Δ in the S layer from its bulk value along the x-axis towards the boundary due to the proximity effect. The scattering times are labeled here as τ_z, τ_x, and τ_{so}, where $\tau_{z(x)}$ corresponds to the magnetic scattering parallel (perpendicular) to the quantization axis and τ_{so} corresponds to the spin-orbit scattering.

In the S layer, the Usadel equations are completed with the self-consistency equation

$$\Delta(x)\ln t + t\sum_{\omega=0}^{\omega=\infty}\left[\frac{2\Delta(x)}{\omega} - \sin\theta_{s1} - \sin\theta_{s2}\right] = 0, \quad (3)$$

where $t = T/T_c$, and T_c is the bulk superconducting temperature. Here and further, we work with the normalized energy parameters $\Delta \equiv \Delta/\pi T_c$, $\omega \equiv \omega/\pi T_c$, $H \equiv H/\pi T_c$; and, for the length parameters in the F layer, $x \equiv x/\xi_n$, $\xi_n = \sqrt{D_f/2\pi T_c}$; and, in the S layer, $x \equiv x/\xi_s$, $\xi_s = \sqrt{D_s/2\pi T_c}$. The scattering parameter notation is $\alpha_z = (\tau_z\pi T_c)^{-1}$, $\alpha_x = (\tau_x\pi T_c)^{-1}$, $\alpha_{so} = (\tau_{so}\pi T_c)^{-1}$. The boundary conditions at the FS interface have the form

$$\gamma_B\frac{\partial\theta_{f1(2)}}{\partial x}\bigg|_{x=-0} = \sin(\theta_{s1(2)} - \theta_{f1(2)}),$$
$$\frac{\gamma_B}{\gamma}\frac{\partial\theta_{s1(2)}}{\partial x}\bigg|_{x=+0} = \sin(\theta_{s1(2)} - \theta_{f1(2)}), \quad (4)$$

and at free edges

$$\frac{\partial\theta_{f1(2)}}{\partial x}\bigg|_{x=-d_f} = 0, \quad \frac{\partial\theta_{s1(2)}}{\partial x}\bigg|_{x=d_s} = 0, \quad (5)$$

where $\gamma = \sigma_n\xi_s/\sigma_s\xi_n$, $\sigma_{n(s)}$ is the conductivity of the F(S) layer, $\gamma_B = R_b\sigma_n/\xi_n$, and R_b is the specific resistance of the SF interface.

For the arbitrary layer thicknesses, the interface parameters (γ, γ_B), and the magnetic scattering parameters, equations (1)–(5) have been solved numerically using the self-consistent two step iterative procedure (for ref. see [1–3]). In the first step, we calculate the order parameter coordinate dependence $\Delta(x)$ using the Matsubara technique using the self-consistent condition in the S layer.

Due to the proximity effect, $\Delta(x)$ decreases towards the SF interface. Then, by proceeding to the analytical extension in (1), (2) over the energy parameter $\omega \longrightarrow -i\varepsilon$ and using the $\Delta(x)$ dependence obtained in the previous step, we find the Green's functions by repeating the iterations until the convergency is reached. The density of states $N(\varepsilon) = N_\uparrow(\varepsilon) + N_\downarrow(\varepsilon)$ can be found as

$$N_{\uparrow(\downarrow)}(\varepsilon) = 0.5N(0)\mathrm{Re}\cos\theta_{1(2)}, \quad (6)$$

where $N_{\uparrow(\downarrow)}$ is the DOS for one spin direction and N is the total DOS.

The numerically obtained energy dependencies of the DOS in the F layer at the free F boundary are presented in Figs. 1–7. At $H = 0$ (Fig. 1), we reproduce the well-known mini gap existing in the SN bilayer [1–3]. The presence of the unixial magnetic scattering tends to smooth the BCS peaks in the DOS. Figure 2 demonstrates the DOS evolution for the spin up electrons for different parameters α_z, where the full black curve corresponds to the usual split peaks within the energy gap due to the exchange field in the absence of any magnetic scattering. By adding the magnetic scattering aligned with the exchange field direction, one can see the smearing of the sharp peaks with the gradual closing of the induced energy gap in the F layer. It is interesting to note that the symmetry of the spin resolved DOS in respect to the Fermi energy ($\varepsilon = 0$) does not exist in the presence of the magnetic scattering.

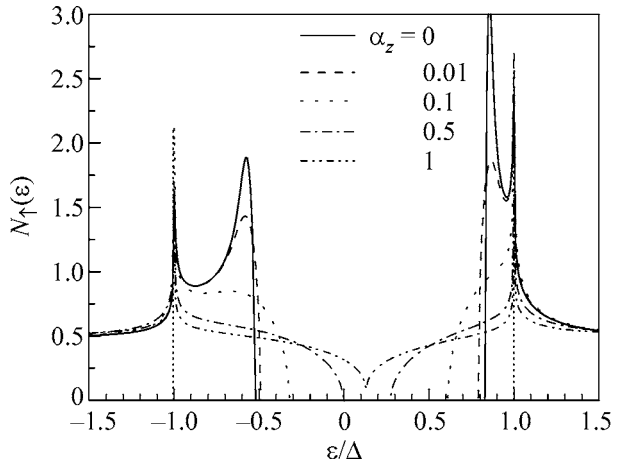

Fig. 2. The case of parallel magnetic scattering. The spin up energy DOS variation in the F layer for several values of the magnetic scattering parameter α_z and for the fixed parameters $H/\pi T_c = 0.2$, $\gamma_B = 5$, $\gamma = 0.05$, $d_f/\xi_n = 0.2$, $d_s/\xi_s = 10$, $\alpha_x = 0$, and $\alpha_{so} = 0$.

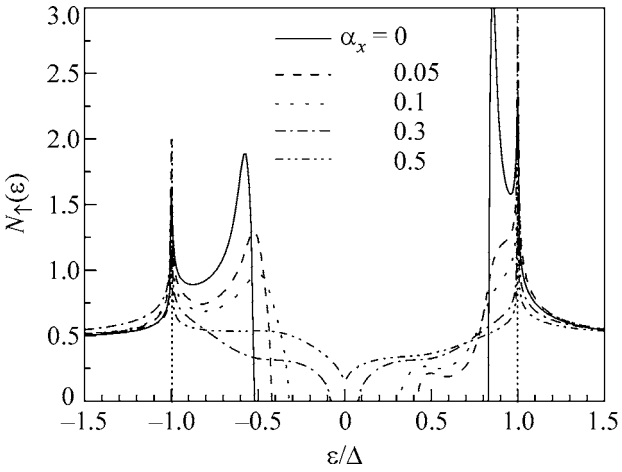

Fig. 3. The case of the perpendicular magnetic scattering. The spin up energy DOS variation in the F layer for several values of the magnetic scattering parameter α_x and for the fixed parameters $H/\pi T_c = 0.2$, $\gamma_B = 5$, $\gamma = 0.05$, $d_f/\xi_n = 0.2$, $d_s/\xi_s = 10$, $\alpha_z = 0$, and $\alpha_{so} = 0$.

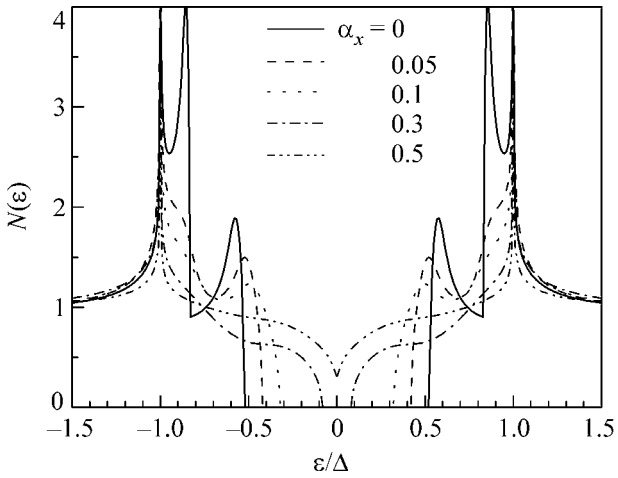

Fig. 4. The case of the perpendicular magnetic scattering. The total DOS energy variation in the F layer for several values of the magnetic scattering parameter α_x and for the fixed parameters $H/\pi T_c = 0.2$, $\gamma_B = 5$, $\gamma = 0.05$, $d_f/\xi_n = 0.2$, $d_s/\xi_s = 10$, $\alpha_z = 0$, and $\alpha_{so} = 0$.

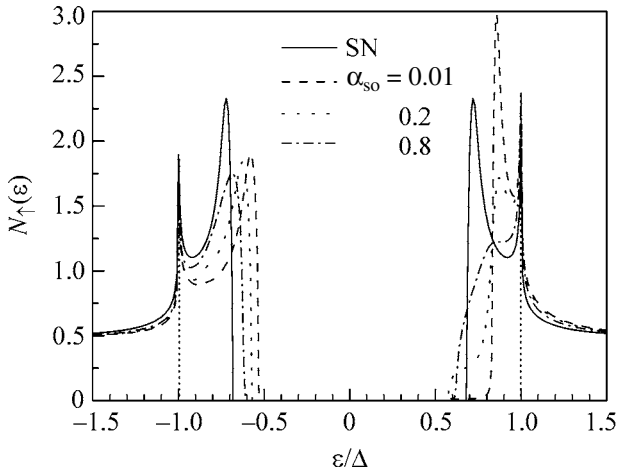

Fig. 5. The case of spin-orbit scattering. The spin up energy DOS variation in the F layer for several values of the magnetic scattering parameter α_{so} and for the fixed parameters $H/\pi T_c = 0.2$, $\gamma_B = 5$, $\gamma = 0.05$, $d_f/\xi_n = 0.2$, $d_s/\xi_s = 10$, $\alpha_z = 0$, and $\alpha_x = 0$. The black curve corresponds to the SN case.

Figure 3 demonstrates the influence of the perpendicular magnetic scattering on the DOS energy variation within the energy gap. The total DOS for both spin directions for the different values of the perpendicular magnetic scattering parameter x is plotted in Fig. 4. The peaks in the DOS are slowly moving towards the zero energy, which can be explained as the presence of some additional splitting field besides the ordinary exchange field in the ferromagnet. As in the case of parallel magnetic scattering, the peaks are smoothed out and the energy gap disappears. For the small magnetic scattering times τ_z and τ_x, the DOS tends to its bulk value in the fenomagnet.

Figures 5 and 6 depict the spin up and total DOS for different parameters of the spin-orbit scattering, correspondingly. It can be seen that, in contrast to the magnetic scattering described above, the spin-orbit scattering tends to decrease the effect of the peak splitting within the energy gap caused by the ferromagnetic exchange field. The black curves in Figs. 5 and 6 correspond to the zero exchange field (the SN structure case). The smaller the spin-orbit scattering time, the

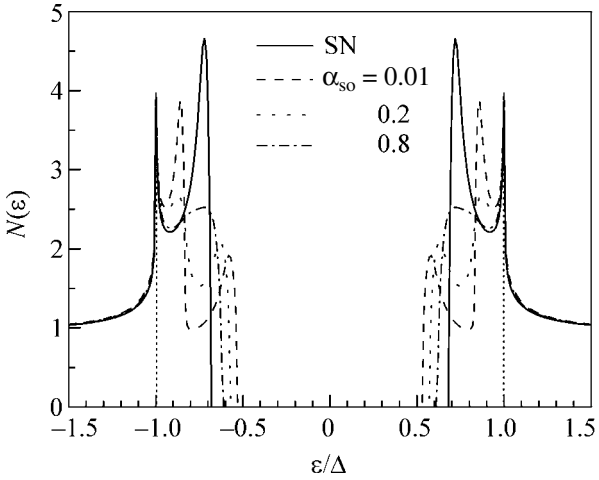

Fig. 6. The case of spin-orbit scattering. The total DOS energy variation in the F layer for several values of the magnetic scattering parameter α_{so} and for the fixed parameters $H/\pi T_c = 0.2$, $\gamma_B = 5$, $\gamma = 0.05$, $d_f/\xi_n = 0.2$, $d_s/\xi_s = 10$, $\alpha_z = 0$, and $\alpha_x = 0$. The black curve corresponds to the SN case.

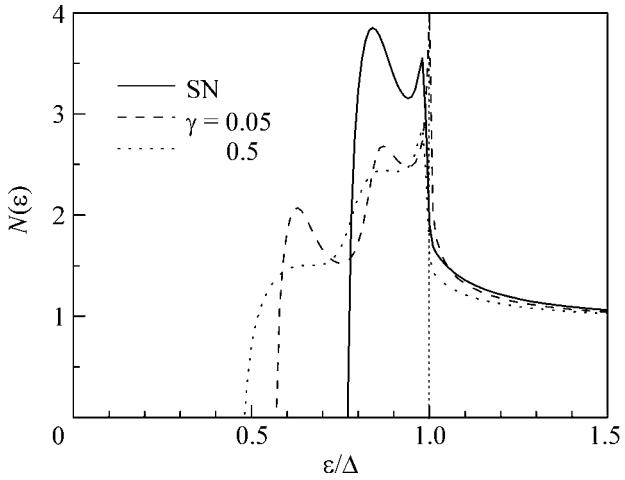

Fig. 7. The case of spin-orbit scattering. The total DOS energy variation in the F layer for $\tau_{so}^{-1} = H$ and for the fixed parameters $H/\pi T_c = 0.2$, $\gamma_B = 5$, $d_f/\xi_n = 0.2$, $d_s/\xi_s = 10$, $\alpha_z = 0$, and $\alpha_x = 0$. The black curve corresponds to the SN case with $\gamma = 0.5$. The dashed and dotted curves correspond to two different values of the γ parameter.

closer the curve to the superconductor/normal metal case, and the two minigap behavior degenerates to the one minigap curve as in the SN structure.

It is interesting to mention the peculiarity of the DOS dependence in the presence of the spin-orbit scattering. As it was shown in [21, 22], in the presence of the spin-orbit scattering for the parameter $\tau_{so}^{-1} = H$, the solution of the Usadel equation changes its characteristic behavior from the oscillating one to a damping decay, which should also cause changes in the DOS energy variation. Figure 7 demonstrates the appearance of a plateau instead of a peak in the DOS for $\tau_{so}^{-1} = H$ for some parameter γ when it is large enough to diminish the penetration of the superconductivity into the F layer. For the particular set of parameters (H, γ_B, d_s, d_f) used for calculation of the graph in Fig. 7, this transformation occurs approximately at $\gamma \approx 0.5$.

Recently, the coexistence of the magnetic and superconducting order in nickel borocarbides was studied in several laboratories experimentally. Such compounds as $ErNi_2B_2C$ and $TmNi_2B_2C$, both being superconducting materials, demonstrate radically different magnetic properties. Local tunneling microscopy at low temperatures revealed a considerable difference in the local superconducting density of states behavior. In contrast with the $TmNi_2B_2C$ [23] compound, where the DOS has its usual BCS type, the $ErNi_2B_2C$ [24] measurements show the nonzero conductance and thereby the nonzero DOS within the energy gap.

To find the possible explanation for such a difference, we propose the following model. We believe that, in the $ErNi_2B_2C$ compound, the magnetic order near the surface is absent even when the antiferromagnetic phase appears in the bulk. This may be related to some atomic compositional disorder near the surface and modified exchange interaction between the magnetic moments near the surface. Consequently, to describe the surface properties of superconducting $ErNi_2B_2C$, the model of a thin film with a relatively strong magnetic scattering on the top of the bulk superconductor without magnetic scattering seems to be quite reasonable.

Using the developed algorithm for the SF bilayer, we may assume the exchange field $H = 0$ as in the paramagnetic case and $\gamma = 1$, $\gamma_B = 0$ for the actual absence of the boundary. Figure 8a demonstrates the calculated DOS behavior at $x = -d_f$ in the presence of the magnetic scattering that destroys the usual BCS behavior. For $ErNi_2B_2C$ having easy plane magnetic anisotropy, we take $1/\tau_z = 0$ and $1/\tau_x = 1/\tau_y = 1/\tau$. Figure 8b corresponds to the case without magnetic scattering. It can be seen that both black theoretical curves are in good agreement with the experimental data of [24] (Figs. 1a and 2b). The difference between the $ErNi_2B_2C$ and $TmNi_2B_2C$ curves may be related to the important difference in their Neel temperatures (6 K and 1.5 K, respectively). The lower T_N may lead to the much smaller magnetic scattering in $TmNi_2B_2C$.

In conclusion, we demonstrated that the increase of spin-orbit or spin-flip electron scattering rates results in completely different transformations of $N(\varepsilon)$ at the free F layer interface. The increase of τ_z^{-1} results in the continuous suppression of the peaks in the density of states accompanied by the closing of the energy gap. The

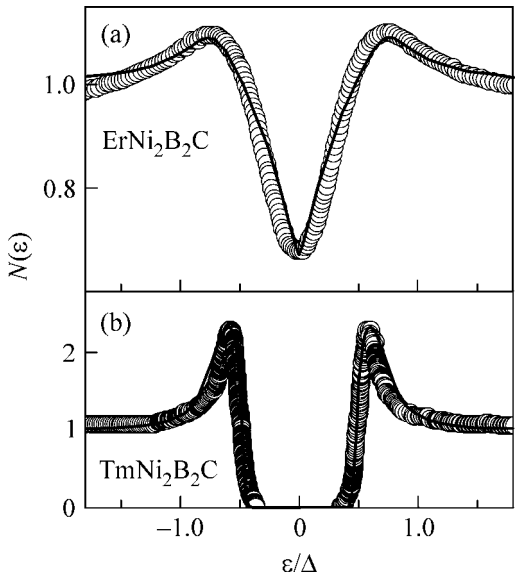

Fig. 8. The theoretical fit of the experimental data of [24] (Fig. 1). The plot parameters are the following: $H = 0$, $\gamma = 1$, $\gamma_B = 0$, $d_s \gg \xi_s$, and $\alpha_z = \alpha_{s0} = 0$; (a) $T = 0.15$ K, $T_c = 11$ K, $d_f = 0.35\xi_n$, and the magnetic scattering parameter $\alpha_x = 0.95$; (b) $T = 0.8$ K, $T_c = 10.5$ K, $d_f = 0.6\xi_n$, and there is no magnetic scattering.

increase of τ_x^{-1} additionally leads to the shift of the peaks towards the zero energy, which looks like the action of some additional exchange field in the ferromagnet. Contrary to that, the increase in τ_{so}^{-1} does not result in the closing of the energy gap and tends to decrease the Zeeman peaks' splitting.

All the calculations have been performed in a self-consistent way in the frame of the Usadel equations. The developed formalism has been successfully applied for the interpretation of the data obtained in the superconductors with the antiferromagnet ordering.

This work was supported by the Russian Foundation for Basic Research (project no. 06-02-90865). We acknowledge the support of the French EGIDE (program no. 10197RC), the ESF Pi-Shift Programme, and the NanoNed programme under project TCS no. 7029. We are grateful to H. Suderow for useful discussions and providing experimental data prior to publication.

REFERENCES

1. A. A. Golubov and M. Yu. Kupriyanov, J. Low Temp. Phys. **70**, 83 (1988).
2. A. A. Golubov and M. Yu. Kupriyanov, Zh. Éksp. Teor. Fiz. **96**, 1420 (1989) [Sov. Phys. JETP **69**, 805 (1989)].
3. A. A. Golubov, E. P. Houwman, J. G. Gijsbertsen, et al., Phys. Rev. B **51**, 1073 (1995).
4. W. Belzig, C. Bruder, and G. Schon, Phys. Rev. B **54**, 9443 (1996).
5. S. Gueron, H. Pothier, N. O. Birge, et al., Phys. Rev. Lett. **77**, 3025 (1996).
6. N. Moussy, H. Courtois, and B. Pannetier, Europhys. Lett. **55**, 861 (2001).
7. E. Scheer, W. Belzig, Y. Naveh, et al., Phys. Rev. Lett. **86**, 284 (2001).
8. L. Cretinon, A. Gupta, B. Pannetier, and H. Courtois, Physica C (Amsterdam) **404**, 103 (2004).
9. A. Buzdin, Rev. Mod. Phys. **77**, 935 (2005).
10. A. A. Golubov, M. Yu. Kuprijanov, and E. Il'ichev, Rev. Mod. Phys. **76**, 411 (2004).
11. F. S. Bergeret, A. F. Volkov, and K. B. Efetov, Rev. Mod. Phys. **77**, 1321 (2005).
12. T. Kontos, M. Aprili, J. Lesueur, and X. Grison, Phys. Rev. Lett. **86**, 304 (2001).
13. L. Cretinon, A. K. Kupta, H. Sellier, et al., Phys. Rev. B **72**, 024511 (2005).
14. S. Reymond, P. SanGiorgio, M. R. Beasley, et al., Phys. Rev. B **73**, 054505 (2006).
15. A. Cottet and W. Belzig, Phys. Rev. B **72**, 180503(R) (2005).
16. C. Cirillo, L. S. Prischepa, M. Salvato, and C. Attanasio, Phys. Rev. B **72**, 144511 (2005).
17. V. A. Oboznov, V. V. Bol'ginov, A. K. Feofanov, et al., cond-mat/0508573.
18. M. Faure, A. I. Buzdin, A. A. Golubov, and M. Yu. Kupriyanov, Phys. Rev. B **73**, 064505 (2006).
19. M. J. DeWeert and G. B. Arnold, Phys. Rev. B **30**, 5048 (1984).
20. M. J. DeWeert, Phys. Rev. B **38**, 732 (1988).
21. E. A. Demler, G. B. Arnold, and M. R. Beasley, Phys. Rev. B **55**, 15 174 (1997).
22. S. Kuplevakhskii and I. Fal'ko, Theor. Mat. Fiz. **86**, 188 (1990).
23. H. Suderow, P. Martinez-Samper, N. Luchier, et al., Phys. Rev. B **64**, 020503(R) (2001).
24. M. Crespo, H. Suderow, S. Vieira, et al., Phys. Rev. Lett. **96**, 027003 (2006).